PNAS RESEARCH ARTICLE | PHYSIOLOGY

WNK kinase is a vasoactive chloride sensor in endothelial cells

Tessa A. C. Garrud[a], Briar Bell[a,b], Alejandro Mata-Daboin[a], Dieniffer Peixoto-Neves[a], Daniel M. Collier[c], Julio F. Cordero-Morales[a,b], and Jonathan H. Jaggar[a,1]

Edited by Fabrice Dabertrand, University of Colorado Anschutz Medical Campus, Aurora, CO; received December 21, 2023; accepted March 1, 2024 by Editorial Board Member Mark T. Nelson

Endothelial cells (ECs) line the wall of blood vessels and regulate arterial contractility to tune regional organ blood flow and systemic pressure. Chloride (Cl^-) is the most abundant anion in ECs and the Cl^- sensitive With-No-Lysine (WNK) kinase is expressed in this cell type. Whether intracellular Cl^- signaling and WNK kinase regulate EC function to alter arterial contractility is unclear. Here, we tested the hypothesis that intracellular Cl^- signaling in ECs regulates arterial contractility and examined the signaling mechanisms involved, including the participation of WNK kinase. Our data obtained using two-photon microscopy and cell-specific inducible knockout mice indicated that acetylcholine, a prototypical vasodilator, stimulated a rapid reduction in intracellular Cl^- concentration ($[Cl^-]_i$) due to the activation of TMEM16A, a Cl^- channel, in ECs of resistance-size arteries. TMEM16A channel-mediated Cl^- signaling activated WNK kinase, which phosphorylated its substrate proteins SPAK and OSR1 in ECs. OSR1 potentiated transient receptor potential vanilloid 4 (TRPV4) currents in a kinase-dependent manner and required a conserved binding motif located in the channel C terminus. Intracellular Ca^{2+} signaling was measured in four dimensions in ECs using a high-speed lightsheet microscope. WNK kinase-dependent activation of TRPV4 channels increased local intracellular Ca^{2+} signaling in ECs and produced vasodilation. In summary, we show that TMEM16A channel activation reduces $[Cl^-]_i$, which activates WNK kinase in ECs. WNK kinase phosphorylates OSR1 which then stimulates TRPV4 channels to produce vasodilation. Thus, TMEM16A channels regulate intracellular Cl^- signaling and WNK kinase activity in ECs to control arterial contractility.

TMEM16A | WNK kinase | TRPV4 | endothelial cell | vasodilation

Significance

Chloride (Cl^-) is the most abundant anion in endothelial cells (ECs). Whether physiological stimuli regulate intracellular Cl^- concentration ($[Cl^-]_i$) in ECs to modify artery contractility is poorly understood. ECs express a Cl^--sensitive kinase termed With-No-Lysine (WNK), but this protein's function in regulating artery contractility is also unclear. Here, we show that acetylcholine, a prototypical vasodilator, activates TMEM16A, a Cl^- channel, leading to a reduction in $[Cl^-]_i$ in ECs. This Cl^- signal activates WNK kinase, which ultimately stimulates transient receptor potential vanilloid 4 (TRPV4) channels on the plasma membrane. Activated TRPV4 channels generate intracellular Ca^{2+} signals in ECs that cause artery relaxation. Thus, TMEM16A channels regulate intracellular Cl^- signaling which controls WNK kinase activity in ECs to modify arterial contractility.

A diverse array of physiological stimuli act via endothelial cells (ECs) to regulate arterial contractility, which controls regional organ blood flow and systemic pressure (1). ECs electrically couple to smooth muscle cells in the arterial wall through gap junctions (2). ECs also produce diffusible vasoactive factors such as nitric oxide (NO), which is a vasodilator (3). Through these intercellular signaling mechanisms, ECs regulate the membrane potential and contractility of arterial smooth muscle cells to control arterial diameter.

Physiological stimuli activate cation channels in ECs to regulate arterial contractility (4). Cation channels which are expressed in ECs include several different transient receptor potential (TRP) channels, including transient receptor potential vanilloid 4 (TRPV4) and small (SK) and intermediate (IK) conductance calcium (Ca^{2+})-activated potassium (K^+) channels (4–6). For instance, acetylcholine (ACh), a muscarinic receptor agonist, activates plasma membrane TRPV4 channels through mechanisms that involve PIP_2 depletion and protein kinase C activation (7, 8). The ensuing Ca^{2+} influx through TRPV4 channels stimulates SK and IK channels to produce membrane hyperpolarization and vasodilation (5, 9). Thus, cation channels exploit the electrochemical gradients of cations to regulate intracellular Ca^{2+} signaling and membrane potential in ECs to control vascular contractility.

ECs also express anion channels, including chloride (Cl^-) channels (10–12). Recent evidence indicates that vasodilators stimulate the anion channel Transmembrane protein 16A (TMEM16A, also termed anoctamin-1) in ECs to produce vasorelaxation (13). This study also demonstrated that vasodilators activate Ca^{2+} influx through surface TRPV4 channels to stimulate nearby TMEM16A channels in ECs (13). However, the mechanisms by which TMEM16A channel activation leads to vasodilation are unclear. Cl^- is the most abundant intracellular and extracellular anion in virtually all cell types. Resting intracellular Cl^- concentration ($[Cl^-]_i$) can vary between approximately 5 and 60 mM depending on cell type (14). $[Cl^-]_i$ is also not static in several cell types and can be modulated by stimuli. Cholinergic agonists rapidly reduced $[Cl^-]_i$ in submandibular salivary gland acinar cells, forskolin, an adenylyl cyclase activator, reduced $[Cl^-]_i$ in guinea pig pancreatic interlobar duct cells, and lectin stimulation increased $[Cl^-]_i$ in human Jurkat T lymphocytes (15–17). Modulation of $[Cl^-]_i$ can also shift signaling by γ-amino butyric acid (GABA) from

Author contributions: T.A.C.G., B.B., A.M.-D., D.P.-N., D.M.C., J.F.C.-M., and J.H.J. designed research; T.A.C.G., B.B., A.M.-D., D.P.-N., and D.M.C. performed research; T.A.C.G., B.B., A.M.-D., D.P.-N., and D.M.C. analyzed data; and T.A.C.G., D.M.C., J.F.C.-M., and J.H.J. wrote the paper.

The authors declare no competing interest.

This article is a PNAS Direct Submission. F.D. is a guest editor invited by the Editorial Board.

[1]To whom correspondence may be addressed. Email: jjaggar@uthsc.edu.

This article contains supporting information online at https://www.pnas.org/lookup/suppl/doi:10.1073/pnas.2322135121/-/DCSupplemental.

Published April 3, 2024.

inhibition to excitation or vice versa in neurons (14, 18). The concept that physiological stimuli regulate $[Cl^-]_i$ in ECs to regulate arterial contractility does not appear to have been investigated.

Intracellular Cl^- modulates the activity of several proteins, including With-No-Lysine (WNK) kinases, Na^+/HCO_3^- cotransporters (NBCs), and the sulfate anion transporter 1 (SLC26A1) (14, 19, 20). The WNK kinase family is unique in that a cysteine residue exists in place of the catalytic lysine which is located in subdomain II of all other protein kinases (21). Cl^- binds to a conserved pocket within the catalytic site of WNK kinases and inhibits autophosphorylation and thus enzyme activity (21, 22). Conversely, a reduction in $[Cl^-]_i$ activates WNK kinases (22). As such, WNK kinases are intracellular Cl^- sensors (21). The unique amino acid sequence in the catalytic domain of WNK kinases has resulted in the development of highly specific and potent inhibitors, including WNK463 (23). Once activated, WNK kinase phosphorylates two additional kinases: SPS-1 related proline/alanine-rich kinase (SPAK) and oxidative-stress responsive kinase-1 (OSR1) (24). SPAK and OSR1 contain conserved C-terminal domains that bind to interaction motifs (R-F-x-V/I or R-x-F-x-V/I) on target proteins, which they then phosphorylate (25–27). Global knockout of WNK1 is embryonic lethal and associated with defective angiogenesis but can be partially rescued by endothelial-specific WNK1 expression (28). Inhibition of WNK kinase impairs EC sprouting and vessel extension ex vivo and prevents cord formation in human umbilical vein endothelial cells (HUVECs) (24, 29). WNK1 and WNK4 mutations in humans are associated with a severe genetic hypertension termed familial hyperkalemic hypertension (fHHT) (21, 30). Despite evidence that WNK kinase is expressed in ECs and plays a vital role in the vascular system, it is not clear whether intracellular Cl^- concentration and WNK kinase are modulated by physiological stimuli to regulate vascular contractility.

Here, we tested the hypothesis that vasodilators regulate $[Cl^-]_i$ to modulate the WNK kinase pathway and investigated the functional significance of such signaling in ECs. Our data demonstrate that ACh activates TMEM16A channels, leading to a rapid reduction in $[Cl^-]_i$ which stimulates WNK kinase signaling in ECs. WNK kinase activation phosphorylates OSR1 and SPAK and stimulates local intracellular Ca^{2+} signaling through TRPV4 channels in ECs. OSR1 potentiates TRPV4 channels through a kinase-dependent mechanism that requires a conserved binding motif (RSFPV) located in the TRPV4 channel C-terminus. Thus, we show that intracellular Cl^- is a physiological signaling ion which acts through WNK kinase and OSR1 to stimulate TRPV4 channels in ECs to produce vasodilation.

Result

ACh Stimulates TMEM16A Channels to Induce a Rapid Reduction in Intracellular Cl^- Concentration in ECs. To examine the regulation of $[Cl^-]_i$ by a vasodilator, primary-cultured mesenteric artery ECs were loaded with MQAE, a Cl^--quenching fluorescent indicator, and imaged using two-photon microscopy (Fig. 1*A*). ACh stimulated a rapid increase in MQAE fluorescence, which corresponds to a reduction in $[Cl^-]_i$ in ECs (Fig. 1 *B* and *C*). As such, analyzed MQAE data are reported as F_0/F to be consistent with the directional change in $[Cl^-]_i$ (Fig. 1 *B* and *C*). Applying a Cl^--free solution containing tributyltin, a Cl^-/OH^- exchanger blocker, and nigericin, a K^+/H^+ exchanger inhibitor, confirmed that MQAE was reporting $[Cl^-]_i$, as has previously been shown (Fig. 1*C*) (31).

Next, we investigated the regulation of $[Cl^-]_i$ by ACh and the mechanisms involved by studying in situ ECs of resistance-size mesenteric arteries. ACh may reduce $[Cl^-]_i$ through the regulation of plasma membrane Cl^- channels or Cl^- cotransporters. TMEM16A is a Ca^{2+}-activated Cl^- channel which is expressed in both arterial smooth muscle and ECs (11, 32). Global TMEM16A knockout mice ($TMEM16A^{-/-}$) die in utero or shortly after birth and exhibit several phenotypes, including repressed gastrointestinal tract peristalsis and tracheal abnormalities (33, 34). To study the involvement

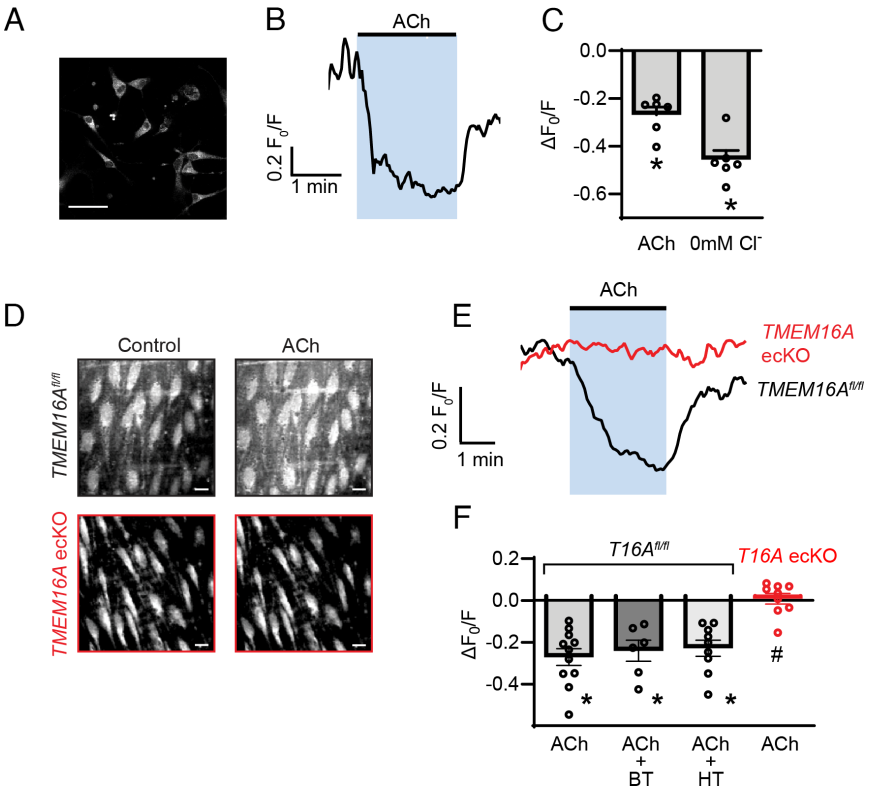

Fig. 1. ACh stimulates a TMEM16A channel-dependent reduction in $[Cl^-]_i$ in ECs. (*A*) MQAE fluorescence in mesenteric artery ECs. (Scale bar, 50 μm.) (*B*) Representative trace illustrating the regulation of MQAE F_0/F by ACh (10 μM) in mesenteric artery ECs. (*C*) Mean data, n = 6 recordings, average 15 cells per recording, * ACh vs. control ($P = 0.0022$), * 0 mM Cl^- vs. control ($P = 0.0022$), two-sided Mann–Whitney *U* test. (*D*) MQAE fluorescence in in situ ECs of *en face* $TMEM16A^{fl/fl}$ and *TMEM16A* ecKO arteries in control and ACh (10 μM). (Scale bar, 10 μm.) (*E*) Representative traces of MQAE F_0/F and regulation by ACh (10 μM) in *en face* mesenteric artery ECs of $TMEM16A^{fl/fl}$ and *TMEM16A* ecKO mice. (*F*) Mean data for regulation of MQAE F_0/F by ACh (10 μM) in $TMEM16A^{fl/fl}$ ECs control and in the presence of bumetanide (BT, 10 μM, 10 min) or hydrochlorothiazide (HT, 10 μM, 10 min) and in *TMEM16A* ecKO ECs. * indicates vs. control ($P < 0.0001$ $TMEM16A^{fl/fl}$, $P = 0.0022$ $TMEM16A^{fl/fl}$ +BT, $P < 0.0001$ $TMEM16A^{fl/fl}$ + HT, $P = 0.2235$ *TMEM16A* ecKO), # indicates vs. $TMEM16A^{fl/fl}$ ($P < 0.0001$ *TMEM16A* ecKO), two-sided Mann–Whitney *U* test, $TMEM16A^{fl/fl}$ n = 11, $TMEM16A^{fl/fl}$ + BT n = 6, $TMEM16A^{fl/fl}$ + HT n = 9, *TMEM16A* ecKO n = 9.

of TMEM16A channels in ECs, we measured $[Cl^-]_i$ in *en face* mesenteric arteries from tamoxifen-inducible EC-specific TMEM16A knock out mice (*TMEM16A* ecKO) and their genetic controls (*TMEM16A*$^{fl/fl}$). TMEM16A channel protein in mesenteric arteries of *TMEM16A* ecKO mice was ~69.9% of that in arteries of *TMEM16A*$^{fl/fl}$ mice, consistent with knockout in ECs (*SI Appendix*, Fig. S1 *A* and *B*) (13). ACh rapidly increased MQAE fluorescence in ECs of *TMEM16A*$^{fl/fl}$ mouse arteries, which corresponds to a reduction in $[Cl^-]_i$, supporting the data obtained in isolated ECs (Fig. 1 *D*–*F*). In contrast, ACh did not reduce $[Cl^-]_i$ in ECs of *TMEM16A* ecKO mouse arteries (Fig. 1 *D*–*F*). Bumetanide, a $Na^+/K^+/Cl^-$ cotransporter (NKCC) inhibitor, or hydrochlorothiazide, a Na^+/Cl^- cotransporter (NCC) inhibitor, did not alter the ACh-induced reduction in $[Cl^-]_i$ in ECs of *TMEM16A*$^{fl/fl}$ mice (*SI Appendix*, Fig. S2*A* and Fig. 1*F*). Bumetanide or hydrochlorothiazide alone also did not alter $[Cl^-]_i$ in ECs (*SI Appendix*, Fig. S2*B*). Following the removal of ACh, MQAE fluorescence partially recovers, suggesting that Cl^- reenters ECs and that the ACh-induced reduction in $[Cl^-]_i$ is reversible (Fig. 1 *B* and *E* and *SI Appendix*, Fig. S2*A*). Bumetanide or hydrochlorothiazide did not alter the recovery of MQAE fluorescence after the washout of ACh (*SI Appendix*, Fig. S2 *A* and *C*). These data indicate that ACh promotes a rapid reduction in $[Cl^-]_i$ through the activation of TMEM16A channels in ECs.

TMEM16A Channels Regulate $[Cl^-]_i$ to Control WNK Kinase Signaling in ECs. We tested the hypothesis that an ACh-induced reduction in $[Cl^-]_i$ regulates WNK kinase activity in ECs. Four WNK isoforms (WNK1-4) exist, with WNK1 predominant in ECs (21, 24, 28). Western blotting detected WNK1, OSR1, and SPAK protein in mesenteric artery ECs (Fig. 2*A*). WNK kinase activation is commonly measured through the phosphorylation of its substrate proteins OSR1 and SPAK (27). We measured the phosphorylation status of the WNK phosphorylation sites Ser 325 on OSR1 (p-OSR1) and Ser 373 on SPAK (p-SPAK) relative to total OSR1 and SPAK, respectively. ACh increased p-OSR1 and p-SPAK in ECs to ~194.1% and 163.7% of controls, respectively (Fig. 2 *A* and *B*). A reduction in extracellular $[Cl^-]$ from 125 to 9 mM also increased p-OSR1 and p-SPAK in ECs to ~375.8% and 248.2% of controls, respectively (Fig. 2 *C* and *D*). The increase in p-OSR1 and p-SPAK by ACh or a decrease in extracellular $[Cl^-]$ were both blocked by a low nanomolar concentration of WNK463, a highly specific and potent WNK kinase inhibitor

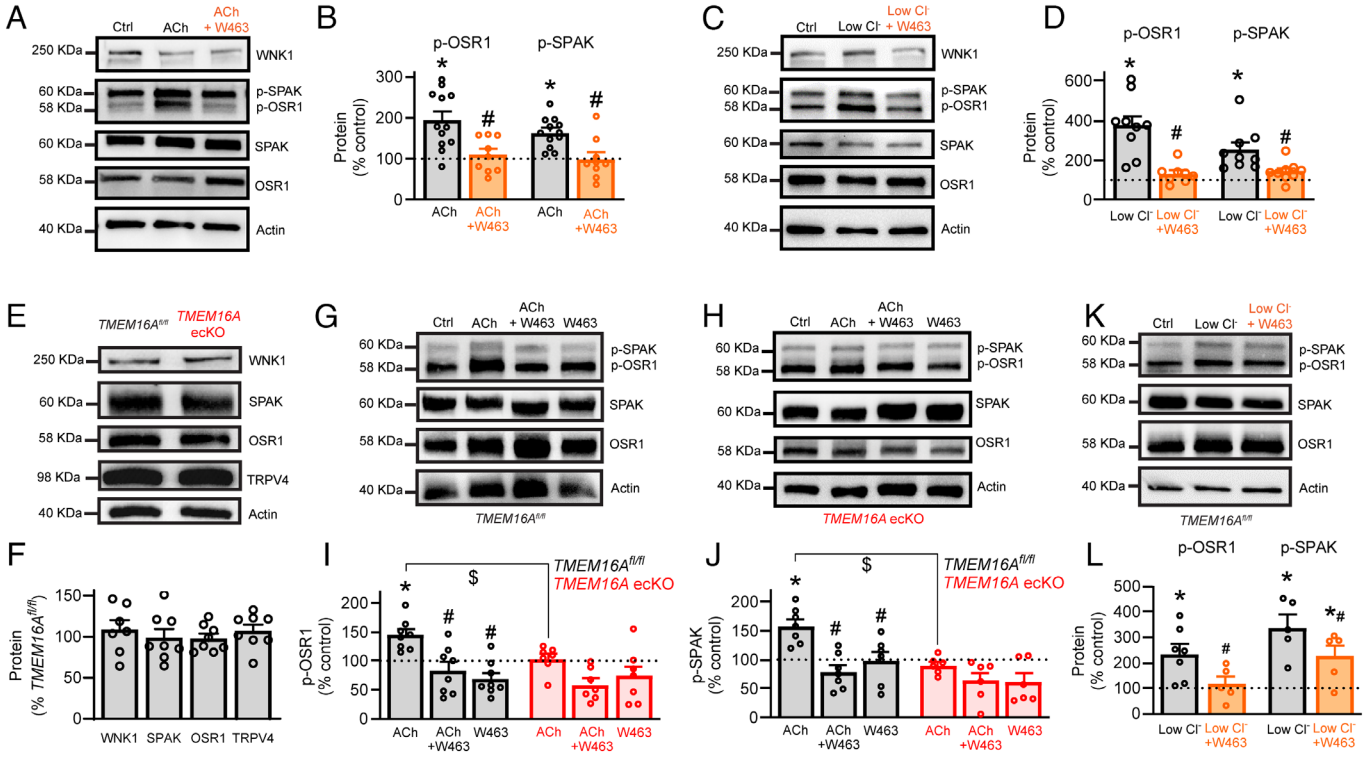

Fig. 2. TMEM16A channels regulate $[Cl^-]_i$ to control WNK kinase signaling in ECs. (*A*) Representative Western blots of WNK1, p-SPAK, p-OSR1, SPAK, OSR1, and actin in mesenteric artery ECs in control (Ctrl), ACh (10 μM, 1 min), and ACh (10 μM, 1 min) + WNK463 (W463, 30 nM, 20 min). (*B*) Mean data for experiments shown in panel *A*. p-OSR1 and p-SPAK were each normalized to their total protein. * vs. control ($P = 0.0012$ ACh p-OSR1, $P = 0.0011$ ACh p-SPAK), # vs. ACh ($P = 0.0145$ ACh + W463 p-OSR1, $P = 0.0005$ ACh + W463 p-SPAK), Kruskal–Wallis Test, ACh p-OSR1 n = 12, ACh + W463 p-OSR1 n = 9, ACh p-SPAK n = 12, ACh + W463 p-SPAK n = 9. (*C*) Representative Western blots of WNK1, p-SPAK, p-OSR1, SPAK, OSR1, and actin in mesenteric artery ECs in control (Ctrl), low Cl^- PSS (9 mM Cl^-, 10 min), and low Cl^- PSS (9 mM Cl^-, 10 min) with WNK463 (W463, 30 nM, 20 min). (*D*) Mean data for *C*. p-OSR1 and p-SPAK were each normalized to their total protein. * vs. control ($P < 0.0001$ low Cl^- p-OSR1, $P < 0.0001$ low Cl^- p-SPAK), # vs. low Cl^- ($P = 0.0142$ low Cl^- + W463 p-OSR1, $P = 0.0430$ low Cl^- + W463 p-SPAK), Kruskal–Wallis test, low Cl^- p-OSR1 n = 9, low Cl^- + W463 p-OSR1 n = 8, low Cl^- p-SPAK n = 9, low Cl^- + W463 p-SPAK n = 9. One outlier was removed after performing a ROUT test. (*E*) Representative Western blots of total WNK1, SPAK, OSR1, TRPV4, and actin proteins in *TMEM16A*$^{fl/fl}$ and *TMEM16A* ecKO mesenteric arteries. (*F*) Mean data for experiments in panel *E* (WNK1 n = 7, SPAK n = 8, OSR1 n = 8, TRPV4 n = 8). (*G*) Representative Western blots of protein from *TMEM16A*$^{fl/fl}$ mesenteric arteries illustrating phosphorylation of OSR1 and SPAK in response to ACh (10 μM, 5 min), with or without WNK463 (30 nM). (*H*) Representative Western blots of protein from *TMEM16A* ecKO mesenteric arteries illustrating phosphorylation of OSR1 and SPAK in response to ACh (10 μM, 5 min), with or without WNK463 (30 nM). (*I*) Mean data for p-OSR1, * vs. control ($P = 0.0429$ ACh *TMEM16A*$^{fl/fl}$), # vs. ACh in *TMEM16A*$^{fl/fl}$ ($P = 0.0157$ ACh + W463 *TMEM16A*$^{fl/fl}$, $P = 0.0004$ W463 *TMEM16A*$^{fl/fl}$) $ indicates comparison between *TMEM16A*$^{fl/fl}$ and *TMEM16A* ecKO ($P = 0.0037$), Kruskal–Wallis test for within genotype testing, Mann–Whitney *U* test for *TMEM16A*$^{fl/fl}$ vs. *TMEM16A* ecKO, *TMEM16A*$^{fl/fl}$ n = 8 each group, *TMEM16A* ecKO n = 7 each group. (*J*) Mean data for p-SPAK, * vs. control ($P = 0.0243$ ACh *TMEM16A*$^{fl/fl}$), # vs. ACh in *TMEM16A*$^{fl/fl}$ ($P = 0.0018$ ACh + W463 *TMEM16A*$^{fl/fl}$, $P = 0.0485$ W463 *TMEM16A*$^{fl/fl}$), $ between *TMEM16A*$^{fl/fl}$ and *TMEM16A* ecKO ($P = 0.0012$), Kruskal–Wallis test for within genotype testing, Mann–Whitney *U* test for *TMEM16A*$^{fl/fl}$ vs. *TMEM16A* ecKO, *TMEM16A*$^{fl/fl}$ n = 7 each group, *TMEM16A* ecKO n = 6 each group. (*K*) Representative Western blots of p-SPAK, p-OSR1, SPAK, OSR1, and actin in control (Ctrl), low Cl^- PSS (9 mM Cl^-, 10 min), or low Cl^- PSS (9 mM Cl^-, 10 min) + WNK463 (W463, 30 nM, 20 min) in mesenteric arteries of *TMEM16A*$^{fl/fl}$ mice. (*L*) Mean data for *K*, * vs. control ($P = 0.0033$ low Cl^- p-OSR1, $P = 0.0063$ low Cl^- p-SPAK), # vs. low Cl^- ($P = 0.0033$ low Cl^- + W463 p-OSR1), Control p-OSR1 n = 7, low Cl^- p-OSR1 n = 7, low Cl^- + W463 p-OSR1 n = 5, p-SPAK n = 5 all groups.

(Fig. 2 *B* and *D*). Exposure to ACh or low Cl^- PSS with or without WNK463 did not alter total OSR1 or SPAK protein levels (*SI Appendix*, Fig. S3 *A* and *B*).

Western blotting was used to measure the regulation of OSR1 and SPAK phosphorylation by EC TMEM16A channels in mesenteric arteries. First, we examined whether the expression of proteins which are involved in WNK1 kinase and TMEM16A channel signaling were altered in mesenteric arteries of *TMEM16A* ecKO mice. WNK1, OSR1, SPAK, and TRPV4 channel proteins were all similar in *TMEM16A*$^{fl/fl}$ and *TMEM16A* ecKO arteries (Fig. 2 *E* and *F*). ACh increased p-OSR1 and p-SPAK phosphorylation to ~144.7% and 158.5% of controls, respectively, in *TMEM16A*$^{fl/fl}$ mesenteric arteries (Fig. 2 *G–J*). WNK463 blocked the ACh-induced increase in p-OSR1 and p-SPAK in *TMEM16A*$^{fl/fl}$ arteries (Fig. 2 *G*, *I*, and *J*). In contrast, ACh did not increase p-SPAK or p-OSR1 and there was no effect of WNK463 in *TMEM16A* ecKO arteries (Fig. 2 *H–J*). Consistent with TMEM16A channels signaling to WNK kinase through a reduction in $[Cl^-]_i$, a reduction in extracellular $[Cl^-]$ from 125 to 9 mM increased p-OSR1 and p-SPAK to ~234.8% and 338.2% of controls, respectively, in mesenteric arteries of *TMEM16A*$^{fl/fl}$ mice (Fig. 2 *K* and *L*). WNK463 inhibited the low $[Cl^-]$-induced increase in p-OSR1 and p-SPAK (Fig. 2 *K* and *L*). These data indicate that ACh stimulates a TMEM16A channel-mediated reduction in $[Cl^-]_i$ which activates WNK kinase, leading to the phosphorylation of both OSR1 and SPAK in ECs of mesenteric arteries.

ACh Stimulates Intracellular Ca^{2+} Signaling in ECs via a TMEM16A Channel- and WNK Kinase-dependent Pathway. Ca^{2+} is a principal second messenger in virtually all cell types, including in ECs (35). ACh binds to muscarinic receptors, which activates surface TRPV4 channels and endoplasmic reticulum inositol 1,4,5 trisphosphate receptors, leading to an increase in intracellular Ca^{2+} signaling in ECs (4). The concept that TMEM16A channels and WNK kinase contribute to agonist-induced Ca^{2+} signaling in ECs does not appear to have been explored. Therefore, the regulation of intracellular Ca^{2+} signaling by TMEM16A channels and WNK kinase was investigated. To measure intracellular Ca^{2+} signals in ECs, we generated *Salsa6f:ecCre+* (ec*Salsa6f*) and *Salsa6f:TMEM16A*$^{fl/fl}$:ecCre+ (*TMEM16A* ecKO-ec*Salsa6f*) mice. Tamoxifen treatment activates EC-specific expression of Salsa6f, a ratiometric Ca^{2+} biosensor composed of GCaMP6f and tdTomato, in both mouse models (Fig. 3 *A* and *B* and Movies S1 and S2). Tamoxifen treatment also knocks out TMEM16A channel

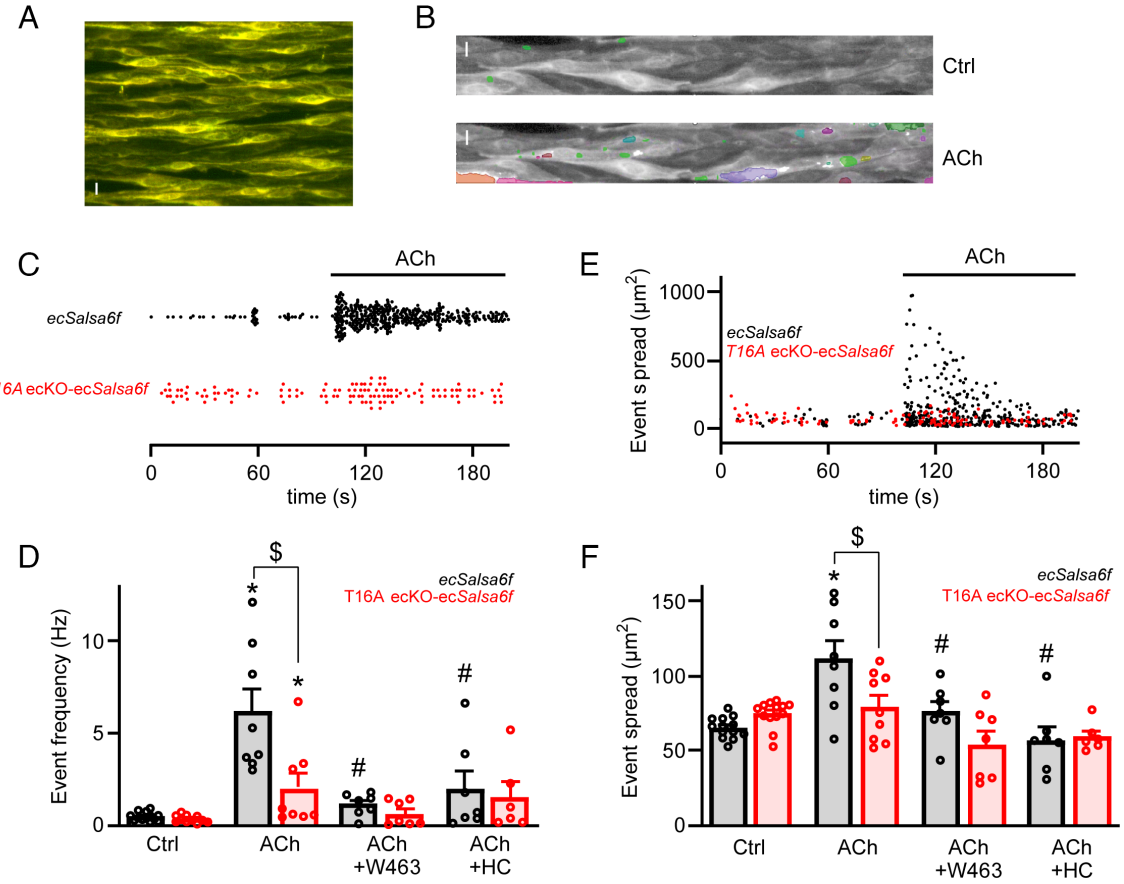

Fig. 3. ACh stimulates intracellular Ca^{2+} signaling in a TMEM16A, TRPV4, and WNK kinase-dependent manner in ECs. (*A*) Maximum z-projection image of GCaMP6f and tdTomato fluorescence (overlay) in ECs of an *en face* mesenteric artery from a ec*Salsa6f* mouse. (Scale bar, 10 µm.) (*B*) Example maximum z projection images of GCaMP6f fluorescence in control (Ctrl) and ACh (10 µM) in the same ECs of a ec*Salsa6f* mouse artery. Colored regions illustrate AI detection of individual Ca^{2+} signals at a single time point. (Scale bar, 10 µm.) (*C*) Representative traces of Ca^{2+} signals that occurred in ECs in control and ACh (10 µM) in an ec*Salsa6f* and *TMEM16A* ecKO-ec*Salsa6f* artery. Each dot represents the occurrence of a Ca^{2+} signal at its corresponding time point. (*D*) Mean data for Ca^{2+} signal frequency measured over 60 s in ECs in control or ACh (10 µM), with or without HC067047 (1 µM) or WNK463 (W463, 30 nM), * vs. control ($P < 0.001$ ACh ec*Salsa6f*, $P = 0.0421$ ACh *TMEM16A* ecKO-ec*Salsa6f*), # vs. ACh ($P = 0.0016$ ACh + HC ec*Salsa6f*, $P = 0.0002$ ACh + W463 ec*Salsa6f*), $ ec*Salsa6f* vs. *TMEM16A* ecKO-ec*Salsa6f* ($P = 0.0078$) for ec*Salsa6f* n = 13 control, n = 8 ACh, n = 7 ACh + HC, n = 7 ACh + WNK463, one-way ANOVA, for *TMEM16A* ecKO-ec*Salsa6f* n = 11 control, n = 8 ACh, n = 6 ACh + HC, n = 7 ACh + W463, Kruskal–Wallis test, Mann–Whitney *U* test for ec*Salsa6f* vs. *TMEM16A* ecKO-ec*Salsa6f*. (*E*) Representative trace of Ca^{2+} signal spatial spread in control and ACh (10 µM) in ECs of a ec*Salsa6f* and *TMEM16A* ecKO-ec*Salsa6f* artery. Each dot represents the spread of one Ca^{2+} signal at its corresponding time point. (*F*) Mean data for Ca^{2+} signal spatial spread over 60 s in ECs in control or ACh (10 µM), with or without HC067047 (1 µM) or WNK463 (W463, 30 nM), * vs. control ($P = 0.0002$ ec*Salsa6f*), # vs. ACh ($P = 0.0001$ ACh + HC ec*Salsa6f*, $P = 0.0141$ ACh + W463 ec*Salsa6f*), $ ec*Salsa6f* vs. *TMEM16A* ecKO-ec*Salsa6f* ($P = 0.0464$).

expression in ECs of the *TMEM16A* ecKO-*ecSalsa6f* mice. Four-dimensional (x, y, and z over time) fluorescent Ca^{2+} imaging was performed in ECs of *en face* mesenteric arteries using a dual inverted selected plane of illumination lightsheet microscope (diSPIM). Advantages of diSPIM over conventional confocal microscopy include that high-resolution (x, 330 nm; y, 330 nm; z, 330 nm) images of the entire cytosolic volume are captured, bleaching of the fluorescent indicator and damage to cells are diminished, and artifacts due to sample movement are abolished as fluorescence is not captured from a thin z-plane (36). In control, the amplitude, duration, frequency, and spatial spread of intracellular Ca^{2+} signals were similar in ECs of ec*Salsa6f* and *TMEM16A* ecKO-ec*Salsa6f* mice (*SI Appendix*, Fig. S4 *A–D* and Movies S1 and S2). ACh increased the frequency of intracellular Ca^{2+} signals ~14.6-fold in ECs of ec*Salsa6f* mice (Fig. 3 *C* and *D* and Movie S1). In contrast, ACh was far less effective at activating Ca^{2+} signals in ECs of *TMEM16A* ecKO-ec*Salsa6f* mice, at ~32.4% of that in ec*Salsa6f* mice (Fig. 3 *C* and *D* and Movie S2). ACh increased the spatial spread of Ca^{2+} signals ~1.7-fold in ECs of ec*Salsa6f* mice but did not alter the spatial spread of Ca^{2+} signals in ECs of *TMEM16A* ecKO-ec*Salsa6f* mice (Fig. 3 *E* and *F*). ACh did not alter Ca^{2+} signal amplitude or duration in ECs of ec*Salsa6f* or *TMEM16A* ecKO-ec*Salsa6f* mice (*SI Appendix*, Fig. S4 *A* and *B*). WNK463 inhibited the ACh-induced increase in Ca^{2+} signaling in ECs of ec*Salsa6f* mice (Fig. 4 *D* and *F*). In contrast, WNK463 did not alter Ca^{2+} signals when applied in the presence of ACh in ECs of *TMEM16A* ecKO-ec*Salsa6f* mice (Fig. 4 *D* and *F*). Similar data were obtained with HC067047, a TRPV4 channel inhibitor, which inhibited the ACh-induced increase in Ca^{2+} signal frequency and spatial spread in ECs of ec*Salsa6f* mice but did not alter Ca^{2+} signals when applied in the presence of ACh in ECs of *TMEM16A* ecKO-ec*Salsa6f* mice (Fig. 3 *D* and *F*). When applied

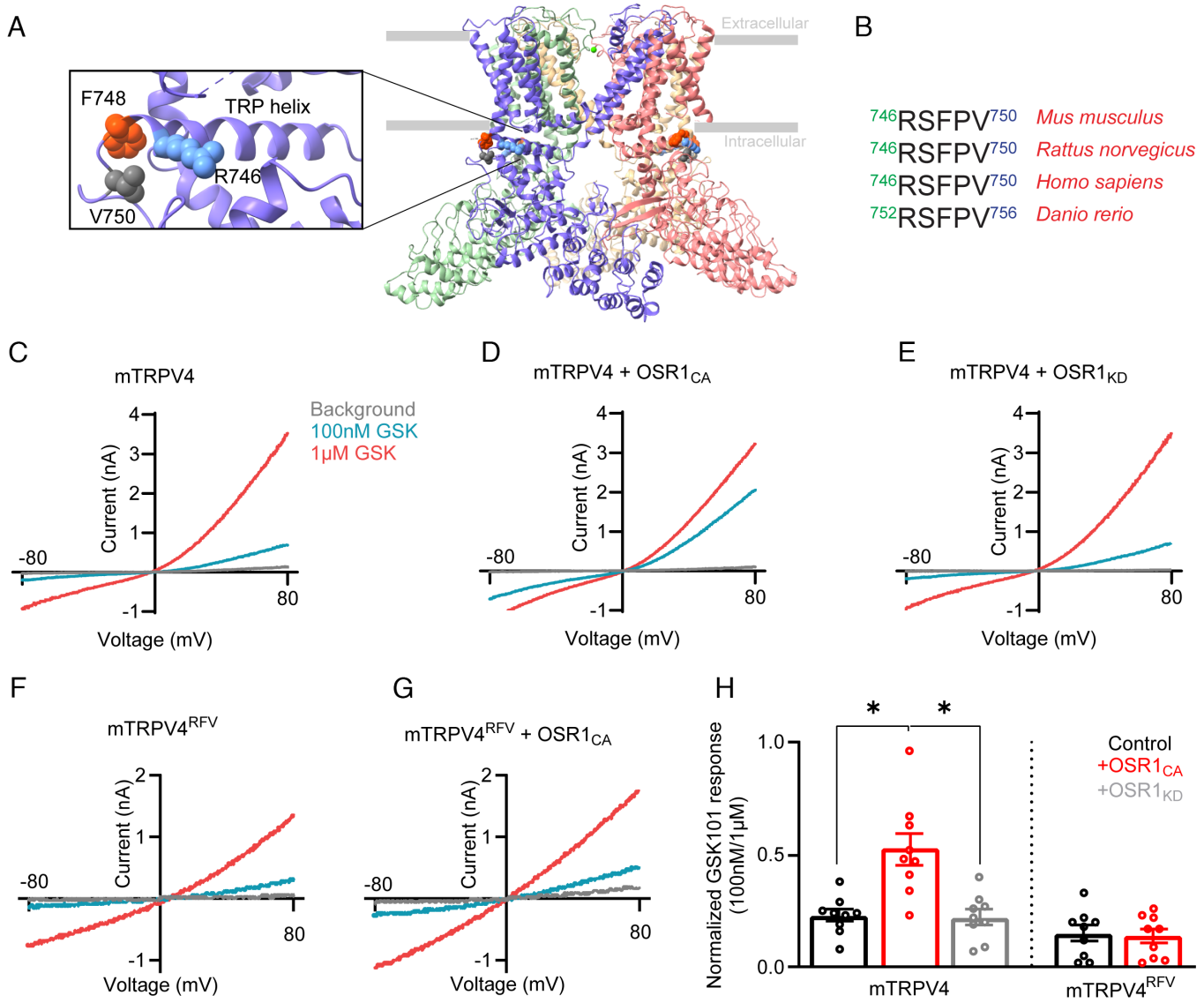

Fig. 4. OSR1 potentiates TRPV4 channels through a conserved binding motif. (*A*) Visualization of the OSR1/SPAK binding site in the TRPV4 channel structure [PDB: 7AA5 (37)]. The conserved amino acids of the RSFPV sequence are highlighted at positions R746, F748, and V750. (*B*) The conserved binding motif is present in multiple species, including mouse (*Mus musculus*), rat (*Rattus norvegicus*), human (*Homo sapiens*), and zebrafish (*Danio rerio*). (*C*) Representative traces of TRPV4 currents measured in HEK293 cells transfected with mouse TRPV4 (mTRPV4) in the presence of no agonist (background), 100 nM GSK101 or 1 μM GSK101. (*D*) Representative traces of TRPV4 currents from HEK293 cells transfected with both mouse TRPV4 and $OSR1_{CA}$. (*E*) Representative traces of TRPV4 currents from HEK293 cells transfected with both mouse TRPV4 and $OSR1_{KD}$. (*F*) Representative traces of TRPV4 currents from HEK293 cells transfected with binding site mutant TRPV4 ($mTRPV4^{RFV}$). (*G*) Representative traces of TRPV4 currents from HEK293 cells transfected with $mTRPV4^{RFV}$ and $OSR1_{CA}$. (*H*) Mean data for normalized GSK101 response ratio (100 nM/1 μM), * was $P = 0.0006$ for mTRPV4 + $OSR1_{CA}$ vs. mTRPV4, and $P = 0.0005$ for mTRPV4 + $OSR1_{KD}$ vs. mTRPV4 + $OSR1_{CA}$, one-way ANOVA, n = 9 all groups.

alone, WNK463 or HC067047 did not alter Ca^{2+} signaling in ECs of ec*Salsa6f* or *TMEM16A* ecKO-ec*Salsa6f* mice (*SI Appendix*, Fig. S4 *C* and *D*).

Experiments were repeated by imaging Cal520, an inorganic fluorescent Ca^{2+} indicator, which was loaded into ECs of mesenteric arteries of *TMEM16A*$^{fl/fl}$ and *TMEM16A* ecKO mice. Similarly to data obtained with ecSalsa6f and *TMEM16A* ecKO-ec*Salsa6f* mice, ACh-induced Ca^{2+} signaling was attenuated in ECs of *en face* mesenteric arteries from *TMEM16A* ecKO mice when compared with arteries of *TMEM16A*$^{fl/fl}$ mice (*SI Appendix*, Fig. S5 *A–C*). WNK463 also inhibited ACh-induced Ca^{2+} signals in ECs of *TMEM16A*$^{fl/fl}$ mice but did not alter Ca^{2+} signaling in the presence of ACh in ECs of *TMEM16A* ecKO mice (*SI Appendix*, Fig. S5 *A–C*). Taken together these data indicate that ACh activates Ca^{2+} signaling in ECs of mesenteric arteries in a TMEM16A, WNK kinase, and TRPV4-dependent manner.

OSR1 Potentiates TRPV4 Currents through a Conserved Binding Motif Located in the Channel C-terminus. SPAK and OSR1 bind to the conserved amino acid sequences R-F-X-V/I or R-X-F-X-V/I in target proteins (26, 38). A protein motif search identified the sequence RSFPV located between amino acids 746 and 750 of the mouse TRPV4 channel C-terminus (Fig. 4*A*). The RSFPV sequence is conserved in TRPV4 channels of species including mouse, rat, human, and zebrafish (Fig. 4*B*). We focused on OSR1 to test the hypothesis that this kinase regulates TRPV4 channels through the RSFPV sequence. Recombinant mouse TRPV4 (mTRPV4) channels were expressed in HEK293 cells either alone, together with constitutively active OSR1 ($OSR1_{CA}$), or with kinase-dead OSR1 ($OSR1_{KD}$). Whole-cell patch-clamp electrophysiology was then used to measure TRPV4 currents elicited by GSK101, a selective TRPV4 channel agonist.

GSK101 produced a concentration-dependent increase in mTRPV4 current amplitude (Fig. 4*C*). Coexpression of $OSR1_{CA}$ increased the ratio of mTRPV4 current generated by 100 nM/1 µM GSK101 to ~227.0% of that in control (Fig. 4 *C*, *D*, and *H*). In contrast, we did not observe this increase with $OSR1_{KD}$ (Fig. 4 *E* and *H*). To determine the functional significance of the RSFPV sequence in TRPV4, all three of the conserved amino acids were mutated to alanine (R746A, F748A, V750A) to produce $mTRPV4^{RFV}$ channels. $mTRPV4^{RFV}$ and mTRPV4 currents were similarly activated by GSK101 (Fig. 4*F*). In contrast to data obtained with mTRPV4 channels, $OSR1_{CA}$ did not increase the activity ratio of $mTRPV4^{RFV}$ channels to GSK101 (Fig. 4 *D*, *G*, and *H*). Next, the minimum requirement in the TRPV4 channel conserved binding motif to facilitate activation by OSR1 was investigated by substituting R746 for alanine ($mTRPV4^{R746A}$). $mTRPV4^{R746A}$ channel activation by GSK 101 was similar to that of both mTRPV4 and $mTRPV4^{RFV}$ channels (*SI Appendix*, Fig. S6*A*). $OSR1_{CA}$ also potentiated $mTRPV4^{R746A}$ channel activation by GSK101 and similarly to that of mTRPV4 channels (*SI Appendix*, Fig. S6 *A–C*). These data suggest that the association of OSR1 with RSFPV in TRPV4 channels is stabilized by other amino acids in the domain. These data indicate that OSR1 enhances TRPV4 function in a kinase-dependent manner that is dependent on the conserved binding motif RSFPV in the TRPV4 channel C-terminus.

WNK Kinase Signaling Amplifies TRPV4 Currents in ECs to Elicit Vasodilation. Ca^{2+} influx through TRPV4 channels activates SK and IK channels in ECs, leading to membrane hyperpolarization and vasodilation (9). We tested the hypothesis that WNK kinase signaling contributes to the regulation of currents in ECs and arterial contractility by TRPV4 and SK/IK channels. Patch-clamp electrophysiology was performed to measure the activation of SK and IK currents by TRPV4 channels in freshly isolated mesenteric artery ECs. Steady-state currents were recorded at −40 mV, a physiological membrane potential, in physiological ionic gradients using the perforated-patch clamp configuration. GSK101 stimulated cell currents that declined to a sustained elevated plateau, consistent with partial desensitization of TRPV4 channels following their activation (Fig. 5*A*) (39). The currents activated by GSK101 were inhibited by a combination of apamin, a SK channel inhibitor, and Tram-34, an IK channel inhibitor, to ~28.3% of those in GSK101 alone (Fig. 5*A*). WNK463 reduced K^+ current activation by GSK101 to ~58.7% of that in the control condition (Fig. 5 *A* and *B*). Furthermore, in the presence of WNK463, apamin+Tram-34 did not inhibit currents activated by GSK101 (Fig. 5 *A* and *C*). These data indicate that WNK kinase signaling increases the activation sensitivity of TRPV4 channels and that the amplification of TRPV4 currents by WNK kinase produces larger IK and SK currents in ECs.

To investigate the regulation of arterial contractility by WNK kinase, we studied pressurized (80 mmHg) resistance-size mesenteric arteries of *TMEM16A*$^{fl/fl}$ and *TMEM16A* ecKO mice. WNK463 did not alter myogenic tone when applied alone, but WNK463 reduced ACh-induced vasodilation to ~20.4% of that in control in *TMEM16A*$^{fl/fl}$ arteries (*SI Appendix*, Fig. S7*A* and Fig. 5 *D–F*). HC067047 also did not alter arterial diameter when applied alone (*SI Appendix*, Fig. S7*B*) but similarly to WNK463 reduced ACh-mediated vasodilation in *TMEM16A*$^{fl/fl}$ arteries (Fig. 5 *D–F*). The coapplication of both WNK463 and HC067047 produced no additional inhibitory effect to when each inhibitor was applied alone (Fig. 5 *D–F*). Apamin+Tram-34 reduced ACh-induced vasodilation to ~32.2% of control (Fig. 5 *G* and *H*). The addition of WNK463 did not further inhibit ACh-induced vasodilation beyond that of apamin+Tram-34 (Fig. 5 *G* and *H*). Dilation to ACh in *TMEM16A* ecKO arteries was ~33.6% of that in *TMEM16A*$^{fl/fl}$ arteries (Fig. 5 *E* and *F*). WNK463 or HC067047 did not alter dilation to ACh in *TMEM16A* ecKO arteries (Fig. 5 *E* and *F*). In the presence of L-NNA, an NOS inhibitor, and indomethacin, a cyclooxygenase blocker, WNK463 or EC-specific TMEM16A knockout reduced vasodilation to ACh (*SI Appendix*, Fig. S7*C*). These results support other data here that TMEM16A channel to WNK kinase signaling acts via the EDH pathway and through TRPV4 and IK/SK channels. WNK463 also did not alter vasodilation to sodium nitroprusside, a NO donor, in *TMEM16A*$^{fl/fl}$ arteries, suggesting that WNK kinase does not contribute to the smooth muscle cell-mediated response to NO (Fig. 5 *I* and *J*). Passive diameter, myogenic tone, and constriction to 60 mM K^+ were all similar in arteries of *TMEM16A*$^{fl/fl}$ and *TMEM16A* ecKO mice (*SI Appendix*, Fig. S7 *D–F*). These data indicate that WNK kinase inhibition in arterial smooth muscle cells does not contribute to attenuated responses to ACh nor is smooth muscle cell contractility altered in arteries of the *TMEM16A* ecKO mice. Taken together, these results indicate that ACh activates TMEM16A channels, leading to a reduction in $[Cl^-]_i$ which activates WNK kinase in ECs. WNK kinase activates OSR1, which interacts with and potentiates TRPV4 channels to amplify SK and IK currents and produce a greater vasodilation.

Discussion

Here, we tested the hypothesis that intracellular Cl^- is a signaling anion in ECs which modulates arterial contractility. ACh stimulated TMEM16A channels, which rapidly decreased $[Cl^-]_i$ in ECs of resistance-size arteries. The reduction in $[Cl^-]_i$ activated WNK kinase, which phosphorylated OSR1 and SPAK. OSR1 recognized

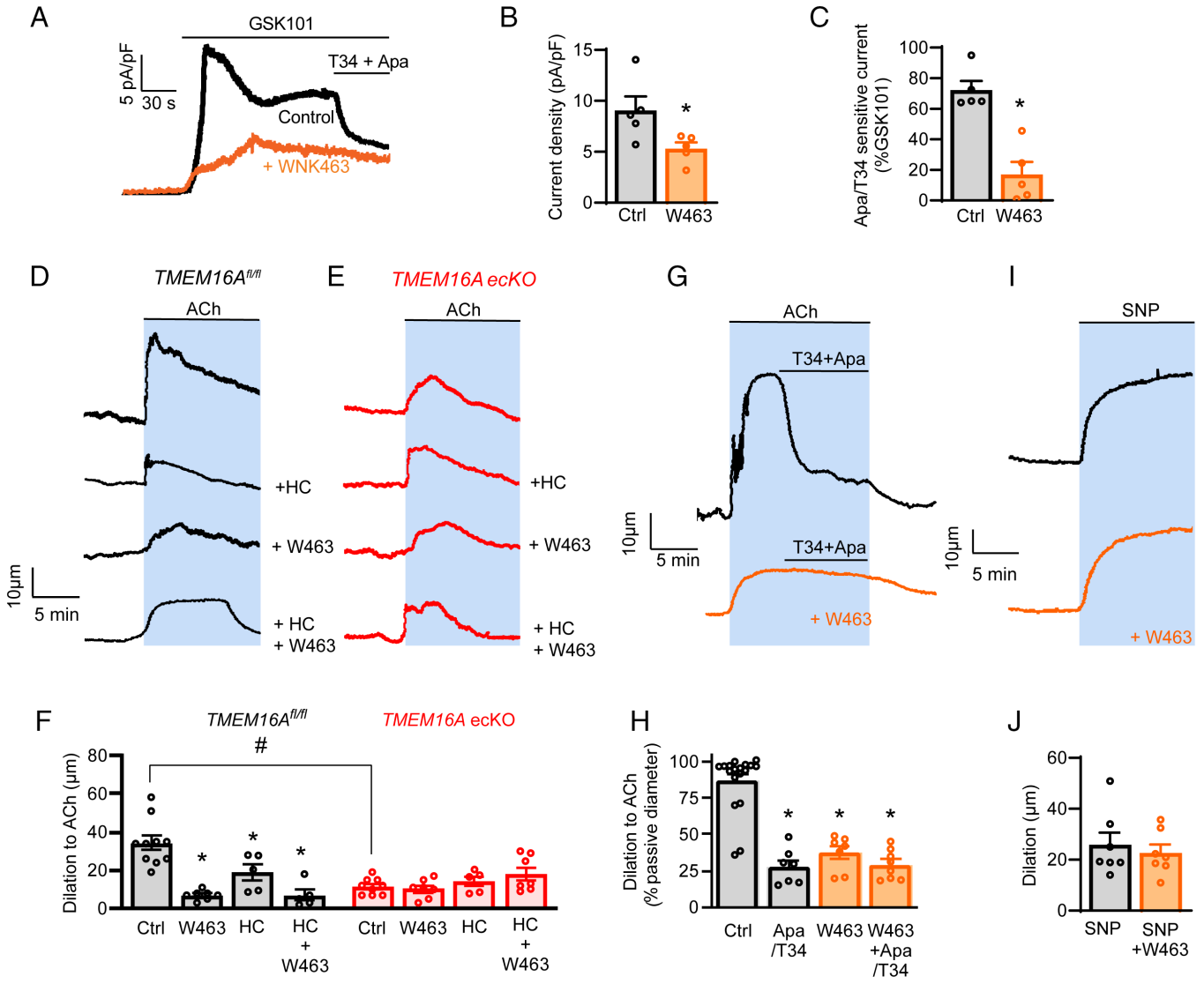

Fig. 5. ACh stimulates vasodilation through TMEM16A channel and WNK kinase activation in ECs. (*A*) Representative traces of currents activated by GSK101 (3 nM) and regulation by apamin (300 nM) and Tram-34 (300 nM), either in control (black) or WNK463 (30 nM, orange) in freshly isolated mesenteric artery ECs. (*B*) Mean data for GSK101-induced current density in control or WNK463, * vs. control ($P = 0.0377$), two-tail *t* test, n = 5 both groups. (*C*) Mean data for apamin/Tram-34 (Apa/T34)-sensitive current in control or WNK463, * vs. control ($P = 0.0006$), two-tail *t* test, n = 5 both groups. (*D*) Representative traces illustrating vasodilation to ACh (10 µM) in control, HC067047 (HC, 1 µM), WNK463 (W463, 30 nM), or HC067047 (HC, 1 µM) + WNK463 (W463, 30 nM) in pressurized (80 mmHg) *TMEM16A*$^{fl/fl}$ and (*E*) *TMEM16A* ecKO arteries. (*F*) Mean data for experiments shown in panels *D* and *E*, * vs. control ($P = 0.0308$ ACh + HC *TMEM16A*$^{fl/fl}$, $P < 0.0001$ ACh + HC/W463 *TMEM16A*$^{fl/fl}$, $P < 0.0001$ ACh + W463 *TMEM16A*$^{fl/fl}$), # for *TMEM16A*$^{fl/fl}$ vs. *TMEM16A* ecKO ($P < 0.0001$) two-way ANOVA with Bonferonni for within genotype testing, *t* test for *TMEM16A*$^{fl/fl}$ vs. *TMEM16A* ecKO, for *TMEM16A*$^{fl/fl}$ n = 10 control, n = 5 HC, n = 5 HC+W463, n = 7 W463, for TMEM16A ecKO n = 9 control, n = 5 HC, n = 7 HC+W463, n = 7 W463. (*G*) Representative traces illustrating vasodilation to ACh (10 µM) with or without W463 (30 nM), with subsequent addition of Tram-34 and apamin (Apa/T34, 300 nM each) in C57BL/6 mouse arteries. (*H*) Mean data for experiments shown in panel *G*, * vs. control ($P = 0.0003$ Apa/T34, $P = 0.0387$ W463, $P = 0.0005$ W463+Apa/T34), Kruskal–Wallis test, n = 18 control, n = 7 Apa/T34, n = 7 W463, n = 8 W463 + Apa/T34. (*I*) Representative traces of vasodilation to sodium nitroprusside (SNP, 10 µM) with or without W463 (30 nM) in the same *TMEM16A*$^{fl/fl}$ artery. (*J*) Mean data for experiments shown in panel *H*, n = 7 both groups.

a conserved RSFPV binding motif on the C-terminus of TRPV4 channels and increased their activity in a kinase-dependent manner. This TMEM16A channel/WNK kinase/TRPV4 channel signaling mechanism stimulated intracellular Ca^{2+} signaling, which activated IK and SK currents in ECs to produce vasodilation. In summary, we show that intracellular Cl^- signaling activates WNK kinase, which through p-OSR1 stimulates TRPV4 channels in ECs to produce vasodilation.

Our data showed that ACh reduced $[Cl^-]_i$ due to the activation of TMEM16A channels in mesenteric artery ECs. Using *TMEM16A* ecKO mice to investigate the functional significance of this channel avoids the effects of pharmacological inhibitors of TMEM16A in both ECs and smooth muscle cells of the intact vascular preparation. These data are consistent with a previous study which showed that carbachol, a muscarinic receptor agonist, reduced $[Cl^-]_i$ in submandibular acinar cells and that this response was absent in cells of global TMEM16A knockout mice (15). The ACh-induced reduction in $[Cl^-]_i$ was partially reversible in *TMEM16A*$^{fl/fl}$ ECs, indicating that Cl^- was transported back into the cytosol. Bumetanide or hydrochlorothiazide did not alter resting $[Cl^-]_i$ over the same time course as did ACh, nor did these NKCC or NCC inhibitors alter the ACh-induced decrease in $[Cl^-]_i$, or the recovery of $[Cl^-]_i$ following the removal of ACh. The recovery of $[Cl^-]_i$ following ACh washout in the presence of an NKCC or KCC inhibitor suggests that either these transporters do not recover $[Cl^-]_i$, the inhibition of one Cl^- cotransporter type

is compensated by another, or that other proteins not studied here, for instance the H^+/Cl^- exchanger, may transport Cl^- into ECs. Our data indicate that ACh did not reduce $[Cl^-]_i$ by inhibiting NKCC1, which is a principal Cl^- influx pathway present in ECs (40). In neurons, NKCC contributes to setting the reversal potential for Cl^- (E_{Cl}) and modifies inhibition by GABA-A receptors ($E_{GABA\text{-}A}$), which are Cl^- channels (14, 18). In rat hippocampal neurons, coincident pre- and postsynaptic activity resulted in a hyperpolarizing shift of E_{Cl} in an NKCC-sensitive manner (18). We have previously shown that ACh-induced local Ca^{2+} influx through TRPV4 channels stimulated nearby TMEM16A channels in ECs (13). When integrating the results here, we conclude that ACh stimulated TRPV4 channels downstream of the muscarinic receptor, leading to Ca^{2+} influx which activated TMEM16A channels, resulting in Cl^- efflux and a reduction in $[Cl^-]_i$ in ECs.

$[Cl^-]_i$ ranges between 5 and 60 mM in a wide variety of different cells, including epithelial, neuronal, and skeletal muscle (14, 16, 41). $[Cl^-]_i$ was 33.2 mM when imaged using 6-methoxy-N-ethylquinolinium iodide (MEQ), a fluorescent Cl^- indicator, in cultured HUVECs (41). The physiological range of membrane potential in pressurized resistance-size arteries is between ~−60 and −32 mV (13, 42). With an extracellular Cl^- concentration of 122 mM, $[Cl^-]_i$ must be more than 11.8 mM at −60 mV and 34.8 mM at −32 mV to drive efflux. WNK kinases are inhibited by $[Cl^-]$ between 5 and 60 mM, with an IC_{50} of ~20 mM (22). MQAE is a single excitation–single emission fluorophore that is not optimal for precise calibration of $[Cl^-]_i$. MQAE fluorescence is linear with $[Cl^-]_i$ less than 40 mM Cl^-, which is a concentration close to what has previously been measured in ECs (31, 41). Genetically encoded ratiometric Cl^- indicators exist, and although their optimum ranges are at higher $[Cl^-]_i$ than MQAE, they are pH-sensitive (43). Given the multiple considerations that must be taken into account when attempting to calibrate $[Cl^-]_i$, we consider that measuring the ACh-induced reduction in $[Cl^-]_i$ in ECs is beyond the scope of this study. Data here strongly indicate that Cl^- efflux through TMEM16A channels activates WNK kinase. We propose that ACh stimulates a millimolar reduction in $[Cl^-]_i$ in ECs.

For Cl^- efflux to occur, counterbalancing cations must also exit cells. K^+ is by far the most highly concentrated intracellular cation at ~140 mM. At physiological membrane potentials, a gradient for K^+ efflux exists (44). ACh-induced TRPV4 channel activation stimulates TMEM16A, SK, and IK channels in ECs (5, 9, 13). Thus, our data suggest that K^+ efflux through SK and IK channels acts as the counterbalance to Cl^- efflux. As the $[K^+]_i$ is far higher than the $[Cl^-]_i$, a relatively small reduction in $[K^+]_i$ would occur, resulting in only a minor impact on the driving force for K^+ through SK/IK channels and their regulation of membrane potential. The resulting membrane hyperpolarization in response to SK/IK activation would augment Ca^{2+} influx through TRPV4 channels and Cl^- efflux through TMEM16A channels to further activate WNK signaling. ACh may drive the membrane potential close to E_{Cl}, although this would depend upon the magnitude of the reduction in $[Cl^-]_i$ and the degree of membrane hyperpolarization. Approaching E_{Cl} would be one mechanism to stabilize the positive feedback loop of this signaling pathway.

Our data demonstrated that ACh and a reduction in extracellular Cl^- stimulated WNK kinase signaling and lead to both OSR1 and SPAK phosphorylation in whole mesenteric arteries and mesenteric artery ECs. OSR1 and SPAK phosphorylation occurred through an EC TMEM16A channel-dependent mechanism. These data indicate that the TMEM16A channel-dependent reduction in $[Cl^-]_i$ stimulates the WNK kinase signaling pathway. TMEM16A channels are expressed and functional in other cell types, including smooth muscle, epithelial, neurons, interstitial cells of Cajal and pericytes (45). Whether TMEM16A channels regulate $[Cl^-]_i$ and WNK kinase signaling to elicit functional effects in cell types other than ECs is unclear but worth investigating. It is possible that ACh may have also activated WNK kinase signaling in ECs through additional mechanisms. Protein kinase B (also termed Akt) activation increased SPAK and OSR1 phosphorylation in the kidneys of db/db hyperinsulinemic mice (46). Akt phosphorylated WNK1 at threonine 58, although it was unclear whether this altered activity, cellular localization, or interaction with other proteins (47). Hyperosmotic stress or ficoll, a molecular crowing agent, also stimulated recombinant WNK1 to form functional liquid-like condensates which activated OSR1 and SPAK (48). Thus, ACh may also regulate WNK kinase signaling through other pathways in ECs.

We did not investigate the WNK kinase family member(s) that mediate the signaling pathway in ECs that we describe here. WNK1 transcript was expressed in HUVECs and human dermal microvascular endothelial cells (HDMECs) and WNK1 protein was detected in HUVECs (24). In contrast, WNK2 and WNK4 transcripts were undetectable in HUVECs (24). We show that WNK1 protein is present in both mesenteric artery ECs and in mesenteric arteries. A shorter kidney-specific WNK1 isoform (KS-WNK1) that is transcribed from exon 4a onward and lacks a functional kinase domain is selectively expressed in the distal convoluted tubule (21). We did not detect a smaller WNK1 band in our Western blots of mesenteric artery lysate, suggesting that KS-WNK1 was absent. WNK3 transcript was detected in HUVECs and HDMECs, but at far lower levels than WNK1 (24). Global or EC-specific WNK1 knockout was embryonic-lethal, highlighting a vital role for WNK1 in ECs (28). In contrast, global WNK3 knockout was not embryonic lethal and was not associated with angiogenesis defects (49). WNK3 knockout mice fed a low-salt diet exhibited lower blood pressure than wild-type mice, although levels of phosphorylated OSR1 and SPAK were unaltered in the kidney and WNK1 and WNK4 proteins were up-regulated, suggesting compensatory mechanisms (49). Future studies should investigate the regulation of arterial contractility by WNK isoforms in ECs.

Conserved C-terminal (CCT) domains in SPAK and OSR1 interact with high affinity to the conserved sequence R-F-x-V which is present in both WNK kinases and target proteins (25–27). Disruption of CCTs prevented phosphorylation of SPAK/OSR1 by WNK kinase or phosphorylation of target proteins by SPAK/OSR1 (25–27). SPAK and OSR1 CCT domains also bind to the variant motif R-x-F-x-V which is present in proteins, including the inward rectifier channels $K_{ir}2.1$ and $K_{ir}2.3$, but not $K_{ir}4.1$ (38). The expression of constitutively active OSR1 increased the density of recombinant $K_{ir}2.1$ currents but did not alter $K_{ir}4.1$ currents, suggesting that this motif is of functional importance (38). We identified the amino acid sequence RSFPV at amino acid positions 746 to 750 in TRPV4 channels. This sequence is located on the C-terminus nearby the TRP domain that runs parallel to the plasma membrane (50). Structural analysis of TRPV4 channels revealed that GSK2798745, an inhibitor, uncoupled the TRP domain from the voltage sensor-like domain, suggesting that this region is important for TRPV4 gating (50). We show that OSR1 kinase activity is essential to increase the sensitivity of mouse TRPV4 currents to GSK101, indicating that channel phosphorylation is likely for this effect. We also found that alanine (A) substitution of the conserved arginine (R), phenylalanine (F), and valine (V) in RSFPV resulted in TRPV4 channels that were insensitive to constitutively active OSR1. These data indicate that OSR1 interacts with TRPV4 channels through the conserved RSFPV

domain. A single alanine substitution at R746 did not prevent the increase of TRPV4 currents by OSR1. These data are similar to those wherein the mutation of either R residue to alanine in RRFIV did not disrupt SPAK and OSR1 binding to a WNK1-derived peptide, whereas the mutation of both R residues did (38). Similarly, all three conserved residues in the R-F-x-V sequence in NKCC1 were required for binding to SPAK/OSR1 CCT domains (25). The residues adjacent to R746 in mouse TRPV4 channels include isoleucine (I744) and aspartic acid (D743). These residues are also present around the arginine residues of the conserved binding motif found in Kir2.1 and Kir2.3 channels, and isoleucine is also near the arginine in conserved sequences located in HSP105 and Gelsolin (26). These residues may provide additional stability for the OSR1-TRPV4 channel interaction (26). We found that the SPAK/OSR1 CCT consensus binding sequences R-F-x-V or R-x-F-x-V/I are not present in TMEM16A, IK, and SK channels. Thus, in this signaling cascade, WNK kinase appears to act solely through the enhancement of TRPV4 channels in ECs.

Consistent with our observations, WNK1 overexpression increased the amplitude of recombinant TRPV4 currents in CHO cells (51). In contrast, WNK1 overexpression reduced recombinant TRPV4 channel surface expression in HEK293 cells (52). WNK-IN-11, a WNK1 inhibitor, also reduced both total and plasma membrane TRPV4 protein in mpkCCD$_{C14}$ cells, an immortalized cortical collecting duct line (51). These earlier findings cannot explain the data presented here as ACh did not alter surface TRPV4 channel abundance in mesenteric arteries over the same time course as it produced vasodilation (5). TRPV4 channel protein was also similar in arteries of *TMEM16A*$^{fl/fl}$ and *TMEM16A* ecKO mice. Thus, data indicate that the interaction of OSR1 with surface TRPV4 and its subsequent phosphorylation increased channel activity in ECs. TRPV4 channels contain several serine/threonine residues which could be phosphorylated by OSR1. For instance, PKA and PKC activation leads to TRPV4 phosphorylation at serine 824, and this has been shown to increase sensitivity to agonists (53, 54). Future studies should identify phosphorylation site(s) for OSR1 in TRPV4 channels. Our results demonstrated that ACh-induced Cl^- signaling also stimulated WNK kinase to phosphorylate SPAK in mesenteric arteries. OSR1 and SPAK are structurally very similar, with their kinase and CCT domains 87% and 78% identical, respectively (26). OSR1 and SPAK share downstream targets and are generally considered to act together (26). However, siRNA-mediated knockdown of SPAK reduced the migration of ECs, whereas knockdown of OSR1 attenuated their proliferation, indicating that there may be some distinctions (24). p-SPAK may also activate TRPV4 channels and this should be investigated in a future study as the participation of both proteins may lead to interesting discoveries regarding their interactions or distinctions.

Acetylcholine (ACh) binds to G_q-coupled M3 receptors and stimulates plasma membrane TRPV4 channels and endoplasmic reticulum IP_3 receptors (9, 55, 56). This results in an increase in $[Ca^{2+}]_i$ which stimulates SK/IK channels and eNOS in ECs, leading to arterial hyperpolarization and vasodilation (3, 5, 9). Here, we show that the inhibition of either WNK kinase or TRPV4 channels similarly reduced ACh-induced Ca^{2+} signaling in ECs. These effects were absent in ECs lacking TMEM16A channels in which ACh did not activate WNK kinase signaling. These results further support our conclusion that TRPV4 channels are a downstream target of TMEM16A-mediated WNK kinase signaling. We have previously shown that ACh stimulates TRPV4 currents, which through Ca^{2+} influx, activate TMEM16A channels in ECs (13). Taken together these data indicate a positive feedback mechanism whereby TRPV4 channels activate TMEM16A channels, leading to WNK kinase signaling which amplifies TRPV4 activity. In accordance with our findings, the treatment of mice with WNK463 for 3 d reduced TRPV4-mediated Ca^{2+} influx in cortical collecting ducts (51). A 24-h treatment with WNK kinase inhibitors also abolished an aldosterone-mediated increase in TRPV4-mediated Ca^{2+} influx in mpkCCD$_{C14}$ cells (51). What initially triggers TRPV4 channel stimulation by ACh is unclear but may involve protein kinase C or PIP_2 depletion (7, 8).

Proteins other than WNK kinases may also be regulated by $[Cl^-]_i$ in ECs. These include Na^+-HCO_3^- cotransporters (NBCs) and the sulfate anion transporter 1 (SLC26A1) (19, 20). A change in $[Cl^-]_i$ has been reported to regulate the activity of other kinases, including c-Jun N-terminal Kinase (JNK), extracellular signal-related kinase (ERK), and serum and glucocorticoid-regulated kinase-1 (SGK1), although in many of these cases, it was not clear whether Cl^- directly or indirectly regulated these proteins (57–59). Efflux of electrolytes may drive water loss and cell shrinkage. However, this is not always the case as changes in $[Cl^-]_i$ occur in GABAergic neurons, but they are relatively insensitive to osmotic stress due to a lack of aquaporin expression (60). ECs of vessels outside of the central nervous system express aquaporin 1 (AQP-1) and loss of AQP-1 is a marker of endothelial dysfunction (61, 62). AQP-3 has also been detected in HUVECs (62). Cl^- loss may or may not lead to a small degree of cell shrinkage in ECs, although cell shrinkage also activates WNK kinase signaling (21). It is beyond the scope of this study to determine whether ACh-induced WNK kinase activation and the reduction in intracellular $[Cl^-]_i$ is associated with a change in cell volume.

Our data lead us to propose a unique positive feedback mechanism for vasodilation (Fig. 6). ACh stimulates TRPV4 channels, leading to Ca^{2+} influx which activates both TMEM16A and SK/IK channels. SK/IK channel activation produces both membrane hyperpolarization and concurrent K^+ and Cl^- efflux through SK/IK and TMEM16A channels, respectively. The reduction in $[Cl^-]_i$ activates WNK kinase, leading to the phosphorylation of

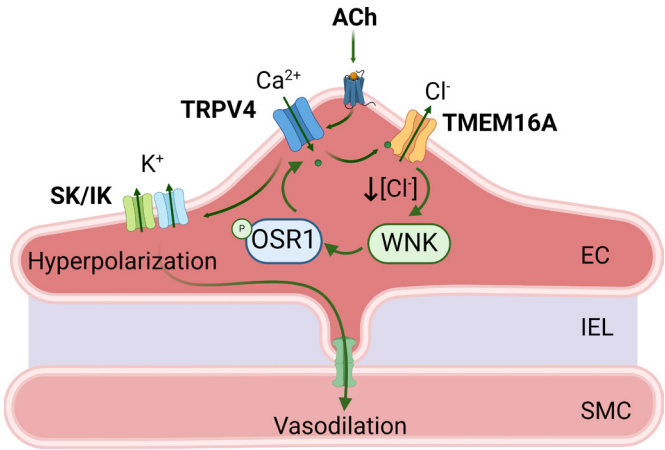

Fig. 6. WNK kinase is a vasoactive Cl^- sensor in ECs. The results of this study lead us to propose the following series signaling cascade regulates arterial contractility: 1) acetylcholine (ACh) binds to muscarinic receptors, which activates TRPV4 channels; 2) Ca^{2+} influx through TRPV4 channels activates TMEM16A channels, resulting in Cl^- efflux and a reduction in $[Cl^-]_i$; 3) the decrease in $[Cl^-]_i$ activates WNK kinase; 4) WNK kinase phosphorylates OSR1, which associates with RSFPV on TRPV4 channels; 5) p-OSR1 increases TRPV4 channel activity through a kinase-dependent mechanism; 6) Ca^{2+} influx through TRPV4 channels is amplified, which further activates IK and SK channels; 7) IK and SK channel activation produces membrane hyperpolarization, which is transmitted to arterial smooth muscle cells through gap junctions, leading to vasodilation. EC, endothelial cell, IEL, internal elastic lamina, SMC, smooth muscle cell.

its substrate protein OSR1, which recognizes a conserved binding motif in TRPV4 channels. p-OSR1 phosphorylates TRPV4 channels and amplifies their activity, which further stimulates TMEM16A, SK and IK channels. A steady-state of this positive feedback loop may involve the membrane potential approaching E_{Cl}, internalization of the muscarinic receptor, or desensitization of TRPV4 channels. Similarly, in vivo arterial diameter is the product of a wide variety of vasoconstrictor and vasodilator stimuli and the pathway we describe likely interacts with others to ensure it is not a runaway process and that an equilibrium is reached.

Here, we describe a unique signaling network between TRPV4, TMEM16A, and SK3/IK channels which is regulated by WNK kinase signaling. We have previously measured the properties and spatial localization of surface TMEM16A, SK3, and TRPV4 clusters in ECs using single molecule localization microscopy (5, 13). Our findings raise questions regarding how WNK kinase signaling impacts the temporal and spatial communication between these proteins in ECs. Many factors will influence signaling between these proteins, including the spatial proximity of individual TRPV4, TMEM16A, and SK3 clusters, the number of TRPV4, TMEM16A, and SK3 channels in individual clusters, the apparent Ca^{2+} sensitivities of TMEM16A, SK3 and IK channels, and the frequency, amplitude and spatial spread of Ca^{2+} sparklets produced by individual TRPV4 clusters. ACh also stimulates SK3 channel anterograde trafficking, which increases the size of surface SK3 clusters that overlap with a TRPV4 cluster in ECs (5). Future studies should aim to investigate the temporal and spatial activation of TMEM16A, SK3, and IK channels by TRPV4 channels and regulation by WNK kinase signaling.

fHHT is associated with mutations in WNK1 and WNK4 in humans (21). Genetic sequencing of families with fHHT found mutations in intron 1 of the WNK1 gene which increased WNK1 expression in the kidney and leukocytes of fHHT patients (30, 63). Studying WNK kinase function in ECs of patients with fHHT may reveal pathological mechanisms associated with the signaling pathway we describe here that contribute to hypertension.

In summary, our data demonstrate that ACh stimulates TMEM16A channels, leading to a reduction in $[Cl^-]_i$ which activates WNK kinase in ECs of resistance size arteries. Through this mechanism, WNK kinase phosphorylates OSR1, which stimulates TRPV4 channels through a conserved binding domain to activate SK and IK channels and induce vasodilation.

Methods

All animal studies were performed in accordance with the Institutional Animal Care and Use Committee (IACUC) at the University of Tennessee Health Science Center. The generation of *TMEM16A*$^{fl/fl}$ mice and *TMEM16A* ecKO mice is described elsewhere (13). *Salsa6f* mice (RRID:IMSR_JAX:031968, ref. 64) and C57BL/6J mice (RRID:IMSR_JAX:000664) were purchased from Jackson Laboratories. *Salsa6f* mice were crossed with either *Cdh5-Cre/ERT2* or *TMEM16A*$^{fl/fl}$:ecCre+ mice to generate *Salsa6f:ecCre+* (ec*Salsa6f*) and *Salsa6f:TMEM16A*$^{fl/fl}$:ecCre+ (*TMEM16A* ecKO-ec*Salsa6f*) mice, respectively. All animal genotypes were confirmed using genomic PCR (Transnetyx, Memphis, TN). Male mice (12 wk) were administered tamoxifen (50 mg/kg, i.p.) for five consecutive days to activate Cre recombinase. Mice were studied 14 to 21 d after the last tamoxifen injection. MQAE was imaged in either primary-cultured mesenteric EC or ECs of *en face* mesenteric arteries using a Zeiss 710 two-photon microscope. Western blotting was performed on primary-cultured mesenteric artery ECs or mesenteric arteries. Intracellular Ca^{2+} signals were imaged in four dimensions at 37 °C in ECs of en face mesenteric arteries from ec*Salsa6f* or *TMEM16A* ecKO-ec*Salsa6f* mice using a diSPIM. Image analysis was performed using Arivis Vision4D and a semantic (pixel-by-pixel) AI deep-learning model. The conventional whole-cell configuration of patch clamp electrophysiology was used to record TRPV4 currents in HEK293 cells. The perforated patch clamp configuration was used to measure currents in freshly isolated ECs. Arterial contractility was measured in pressurized mesenteric arteries using edge-detection myography. Data are presented as mean ± SEM. Normality of data was testing using Kolmogorov–Smirnoff test. For normally distributed data, student's *t* test and ANOVA with Bonferroni or Tukey (for one- or two-way, respectively) post hoc test was used. For non-normally distributed data, Man–Whitney (two groups) or Kruskal–Wallis test (more than two groups) was utilized. ROUT outlier test was performed to identify outliers. All statistical tests were conducted using GraphPad Prism software. $P < 0.05$ was considered significant. Power analysis was performed using G-power software to ensure sample sizes were sufficient.

Expanded Methods are provided in *SI Appendix*.

Data, Materials, and Software Availability. All study data are included in the article and/or supporting information.

ACKNOWLEDGMENTS. This work was supported by NIH/NHLBI grant HL155180 (J.H.J.), NIH/NHLBI grant HL158846 (J.H.J.), NIH/NHLBI grant HL166411 (J.H.J.), NIH/NIGMS grant GM149218 (J.C.-M.), American Heart Association (AHA) Postdoctoral Fellowship AHA 830462 (A.M.-D.), AHA Postdoctoral Fellowship AHA 1014035 (T.A.C.G.).

Author affiliations: [a]Department of Physiology, University of Tennessee Health Science Center, Memphis, TN 38163; [b]Department of Biochemistry and Molecular Biology, McGovern Medical School at The University of Texas Health Science Center at Houston, Houston, TX 77030; and [c]Department of Pharmaceutical Sciences, University of Tennessee Health Science Center, Memphis, TN 38163

1. J. R. Vane, The Croonian Lecture, 1993. The endothelium: Maestro of the blood circulation. *Philos Trans. R Soc. Lond B Biol. Sci.* **343**, 225–246 (1994), 10.1098/rstb.1994.0023.
2. C. J. Garland, C. R. Hiley, K. A. Dora, EDHF: Spreading the influence of the endothelium. *Br. J. Pharmacol.* **164**, 839–852 (2011), 10.1111/j.1476-5381.2010.01148.x.
3. G. Edwards, M. Félétou, A. H. Weston, Endothelium-derived hyperpolarising factors and associated pathways: A synopsis. *Pflugers Arch.* **459**, 863–879 (2010), 10.1007/s00424-010-0817-1.
4. W. F. Jackson, Endothelial ion channels and cell-cell communication in the microcirculation. *Front Physiol.* **13**, 805149 (2022), 10.3389/fphys.2022.805149.
5. D. Peixoto-Neves *et al.*, Vasodilators mobilize SK3 channels in endothelial cells to produce arterial relaxation. *Proc. Natl. Acad. Sci. U.S.A.* **120**, e2303238120 (2023), 10.1073/pnas.2303238120.
6. S. Earley, J. E. Brayden, Transient receptor potential channels in the vasculature. *Physiol. Rev.* **95**, 645–690 (2015).
7. R. K. Adapala *et al.*, PKCα mediates acetylcholine-induced activation of TRPV4-dependent calcium influx in endothelial cells. *Am. J. Physiol. Heart Circ. Physiol.* **301**, H757–H765 (2011), 10.1152/ajpheart.00142.2011.
8. O. F. Harraz, T. A. Longden, D. Hill-Eubanks, M. T. Nelson, PIP2 depletion promotes TRPV4 channel activity in mouse brain capillary endothelial cells. *ELife* **7**, e38689 (2018), 10.7554/eLife.38689.
9. S. K. Sonkusare *et al.*, Elementary Ca^{2+} signals through endothelial TRPV4 channels regulate vascular function. *Science* **336**, 597–601 (2012), 10.1126/science.1216283.
10. B. Nilius, G. Szucs, S. Heinke, T. Voets, G. Droogmans, Multiple types of chloride channels in bovine pulmonary artery endothelial cells. *J. Vasc. Res.* **34**, 220–228 (1997).
11. F. S. Lamb *et al.*, Expression of CLCN voltage-gated chloride channel genes in human blood vessels. *J. Mol. Cell Cardiol.* **31**, 657–666 (1999), 10.1006/jmcc.1998.0901.
12. T. Suzuki *et al.*, TMEM16A Ca^{2+}-activated Cl− channel regulates the proliferation and migration of brain capillary endothelial cells. *Mol. Pharmacol.* **98**, 61–71 (2020), 10.1124/mol.119.118844.
13. A. Mata-Daboin *et al.*, Vasodilators activate TMEM16A channels in endothelial cells to reduce blood pressure. *Sci. Signal.* **16**, eadh9399 (2023), 10.1126/scisignal.adh9399.
14. B. P. Lüscher, L. Vachel, E. Ohana, S. Muallem, Cl− as a bona fide signaling ion. *Am. J. Physiol. Cell Physiol.* **318**, C125–C136 (2020). 10.1152/ajpcell.00354.2019.
15. V. G. Romanenko *et al.*, Tmem16A encodes the Ca^{2+}-activated Cl^- channel in mouse submandibular salivary gland acinar cells. *J. Biol. Chem.* **285**, 12990–13001 (2010), 10.1074/jbc.M109.068544.
16. H. Ishiguro *et al.*, Chloride transport in microperfused interlobular ducts isolated from guinea-pig pancreas. *J. Physiol.* **539**, 175–189 (2002), 10.1113/jphysiol.2001.012490.
17. Z. F. Lai, Y. Z. Chen, K. Nishi, Modulation of intracellular Cl- homeostasis by lectin-stimulation in Jurkat T lymphocytes. *Eur. J. Pharmacol.* **482**, 1–8 (2003), 10.1016/s0014-2999(03)02076-4.
18. T. Balena, M. A. Woodin, Coincident pre- and postsynaptic activity downregulates NKCC1 to hyperpolarize E(Cl) during development. *Eur. J. Neurosci.* **27**, 2402–2412 (2008), 10.1111/j.1460-9568.2008.06194.x.
19. N. Shcheynikov *et al.*, Intracellular Cl- as a signaling ion that potently regulates Na^+/HCO3− transporters. *Proc. Natl. Acad. Sci. U.S.A.* **112**, E329–337 (2015), 10.1073/pnas.1415673112.
20. M. Wu *et al.*, Extracellular Cl(-) regulates human SO_4^{2-}/anion exchanger SLC26A1 by altering pH sensitivity of anion transport. *Pflugers Arch.* **468**, 1311–1332 (2016), 10.1007/s00424-016-1823-8.
21. J. A. McCormick, D. H. Ellison, The WNKs: Atypical protein kinases with pleiotropic actions. *Physiol. Rev.* **91**, 177–219 (2011), 10.1152/physrev.00017.2010.

22. A. T. Piala *et al.*, Chloride sensing by WNK1 involves inhibition of autophosphorylation. *Sci. Signal* **7**, ra41 (2014), 10.1126/scisignal.2005050.
23. K. Yamada *et al.*, Small-molecule WNK inhibition regulates cardiovascular and renal function. *Nat. Chem. Biol.* **12**, 896–898 (2016), 10.1038/nchembio.2168.
24. H. A. Dbouk *et al.*, Actions of the protein kinase WNK1 on endothelial cells are differentially mediated by its substrate kinases OSR1 and SPAK. *Proc. Natl. Acad. Sci. U.S.A.* **111**, 15999–16004 (2014), 10.1073/pnas.1419057111.
25. A. C. Vitari *et al.*, Functional interactions of the SPAK/OSR1 kinases with their upstream activator WNK1 and downstream substrate NKCC1. *Biochem. J.* **397**, 223–231 (2006), 10.1042/bj20060220.
26. C. A. T. Taylor, M. H. Cobb, CCT and CCT-like modular protein interaction domains in WNK signaling. *Mol. Pharmacol.* **101**, 201–212 (2022), 10.1124/molpharm.121.000307.
27. P. de Los Heros *et al.*, The WNK-regulated SPAK/OSR1 kinases directly phosphorylate and inhibit the K^+–Cl^- co-transporters. *Biochem. J.* **458**, 559–573 (2014), 10.1042/bj20131478.
28. J. Xie *et al.*, Endothelial-specific expression of WNK1 kinase is essential for angiogenesis and heart development in mice. *Am. J. Pathol.* **175**, 1315–1327 (2009), 10.2353/ajpath.2009.090094.
29. A. B. Jaykumar *et al.*, WNK1 collaborates with TGF-β in endothelial cell junction turnover and angiogenesis. *Proc. Natl. Acad. Sci. U.S.A.* **119**, e2203743119 (2022), 10.1073/pnas.2203743119.
30. F. H. Wilson *et al.*, Human hypertension caused by mutations in WNK kinases. *Science* **293**, 1107–1112 (2001), 10.1126/science.1062844.
31. N. Marandi, A. Konnerth, O. Garaschuk, Two-photon chloride imaging in neurons of brain slices. *Pflugers Arch.* **445**, 357–365 (2002), 10.1007/s00424-002-0933-7.
32. A. J. Davis *et al.*, Expression profile and protein translation of TMEM16A in murine smooth muscle. *Am. J. Physiol. Cell Physiol.* **299**, C948–C959 (2010), 10.1152/ajpcell.00018.2010.
33. J. R. Rock, C. R. Futtner, B. D. Harfe, The transmembrane protein TMEM16A is required for normal development of the murine trachea. *Dev. Biol.* **321**, 141–149 (2008), 10.1016/j.ydbio.2008.06.009.
34. S. J. Hwang *et al.*, Expression of anoctamin 1/TMEM16A by interstitial cells of Cajal is fundamental for slow wave activity in gastrointestinal muscles. *J. Physiol.* **587**, 4887–4904 (2009), 10.1113/jphysiol.2009.176198.
35. M. J. Berridge, Calcium signal transduction and cellular control mechanisms. *Biochim. Biophys. Acta* **1742**, 3–7 (2004), 10.1016/j.bbamcr.2004.08.012.
36. J. Icha, M. Weber, J. C. Waters, C. Norden, Phototoxicity in live fluorescence microscopy, and how to avoid it. *Bioessays* **39**, 170003 (2017), 10.1002/bies.201700003.
37. M. Botte *et al.*, Human TRPV4 structure in presence of 4a-PDD. Protein Data Bank. https://doi.org/10.2210/pdb7aa5/pdb. Accessed 8 November 2023.
38. C. A. Taylor *et al.*, OSR1 regulates a subset of inward rectifier potassium channels via a binding motif variant. *Proc. Natl Acad. Sci. U.S.A.* **115**, 3840–3845 (2018), 10.1073/pnas.1802339115.
39. M. Jin *et al.*, Determinants of TRPV4 activity following selective activation by small molecule agonist GSK1016790A. *PLoS One* **6**, e16713 (2011), 10.1371/journal.pone.0016713.
40. S. Foroutan, J. Brillault, B. Forbush, M. E. O'Donnell, Moderate-to-severe ischemic conditions increase activity and phosphorylation of the cerebral microvascular endothelial cell Na^+-K^+-Cl^- cotransporte. *Am. J. Physiol. Cell Physiol.* **289**, C1492–C1501 (2005), 10.1152/ajpcell.00257.2005.
41. K. Li *et al.*, Reduced intracellular chloride concentration impairs angiogenesis by inhibiting oxidative stress-mediated VEGFR2 activation. *Acta Pharmacol. Sinica* **42**, 560–572 (2021), 10.1038/s41401-020-0458-7.
42. H. J. Knot, N. B. Standen, M. T. Nelson, Ryanodine receptors regulate arterial diameter and wall [Ca2+] in cerebral arteries of rat via Ca^{2+}-dependent K^+ channels. *J. Physiol.* **508**, 211–221 (1998). 10.1111/j.1469-7793.1998.211br.x.
43. S. Y. Wu, Y. Shen, I. Shkolnikov, R. E. Campbell, Fluorescent indicators for biological imaging of monatomic ions. *Front. Cell Dev. Biol.* **10**, 885440 (2022), 10.3389/fcell.2022.885440.
44. W. F. Jackson, Boosting the signal: Endothelial inward rectifier K^+ channels. *Microcirculation* **24**, e12319 (2017), 10.1111/micc.12319.
45. Q. Ji *et al.*, Recent advances in TMEM16A: Structure, function, and disease. *J. Cell Physiol.* **234**, 7856–7873 (2019), 10.1002/jcp.27865.
46. H. Nishida *et al.*, Phosphatidylinositol 3-kinase/Akt signaling pathway activates the WNK-OSR1/SPAK-NCC phosphorylation cascade in hyperinsulinemic db/db mice. *Hypertension* **60**, 981–990 (2012), 10.1161/hypertensionaha.112.201509.
47. A. C. Vitari *et al.*, WNK1, the kinase mutated in an inherited high-blood-pressure syndrome, is a novel PKB (protein kinase B)/Akt substrate. *Biochem. J.* **378**, 257–268 (2004), 10.1042/bj20031692.
48. C. R. Boyd-Shiwarski *et al.*, WNK kinases sense molecular crowding and rescue cell volume via phase separation. *Cell* **185**, 4488–4506.e20 (2022), 10.1016/j.cell.2022.09.042.
49. K. Oi *et al.*, A minor role of WNK3 in regulating phosphorylation of renal NKCC2 and NCC co-transporters in vivo. *Biol. Open* **1**, 120–127 (2012), 10.1242/bio.2011048.
50. D. H. Kwon *et al.*, TRPV4-Rho GTPase complex structures reveal mechanisms of gating and disease. *Nat. Commun.* **14**, 3732 (2023), 10.1038/s41467-023-39345-0.
51. V. N. Tomilin, K. Pyrshev, N. H. Khayyat, O. Zaika, O. Pochynyuk, With-No-Lysine Kinase 1 (WNK1) augments TRPV4 function in the aldosterone-sensitive distal nephron. *Cells* **10**, 1482 (2021), 10.3390/cells10061482.
52. Y. Fu, A. Subramanya, D. Rozansky, D. M. Cohen, WNK kinases influence TRPV4 channel function and localization. *Am. J. Physiol. Renal Physiol.* **290**, F1305–F1314 (2006), 10.1152/ajprenal.00391.2005.
53. H. Peng *et al.*, Identification of a Protein Kinase C-dependent phosphorylation site involved in sensitization of TRPV4 channel. *Biochem. Biophys. Res. Commun.* **391**, 1721–1725 (2010), 10.1016/j.bbrc.2009.12.140.
54. S. Cao *et al.*, Transient receptor potential vanilloid 4 (TRPV4) activation by arachidonic acid requires protein kinase A-mediated phosphorylation. *J. Biol. Chem.* **293**, 5307–5322 (2018), 10.1074/jbc.M117.811075.
55. J. L. Bény, M. N. Nguyen, M. Marino, M. Matsui, Muscarinic receptor knockout mice confirm involvement of M3 receptor in endothelium-dependent vasodilatation in mouse arteries. *J. Cardiovasc. Pharmacol.* **51**, 505–512 (2008), 10.1097/FJC.0b013e31816d5f2f.
56. X. Wang, F. Lau, L. Li, A. Yoshikawa, C. van Breemen, Acetylcholine-sensitive intracellular Ca2+ store in fresh endothelial cells and evidence for ryanodine receptors. *Circ. Res.* **77**, 37–42 (1995), 10.1161/01.res.77.1.37.
57. Q. Wu *et al.*, Reduction of intracellular chloride concentration promotes foam cell formation. *Circ J.* **80**, 1024–1033 (2016). 10.1253/circj.CJ-15-1209.
58. Y. L. Zhang *et al.*, Increased intracellular Cl^- concentration promotes ongoing inflammation in airway epithelium. *Mucosal. Immunol.* **11**, 1149–1157 (2018). 10.1038/s41385-018-0013-8.
59. R. Ohsawa *et al.*, Intracellular chloride regulates cell proliferation through the activation of stress-activated protein kinases in MKN28 human gastric cancer cells. *J. Cell Physiol.* **223**, 764–770 (2010), 10.1002/jcp.22088.
60. K. T. Kahle *et al.*, K-Cl cotransporters, cell volume homeostasis, and neurological disease. *Trends Mol. Med.* **21**, 513–523 (2015), 10.1016/j.molmed.2015.05.008.
61. A. S. Verkman, Aquaporin water channels and endothelial cell function. *J. Anat* **200**, 617–627 (2002), 10.1046/j.1469-7580.2002.00058.x.
62. I. V. da Silva, M. Barroso, T. Moura, R. Castro, G. Soveral, Endothelial aquaporins and hypomethylation: Potential implications for atherosclerosis and cardiovascular disease. *Int. J. Mol. Sci.* **19**, 130 (2018), 10.3390/ijms19010130.
63. E. Vidal-Petiot *et al.*, WNK1-related Familial Hyperkalemic Hypertension results from an increased expression of L-WNK1 specifically in the distal nephron. *Proc. Natl. Acad. Sci. U.S.A.* **110**, 14366–14371 (2013), 10.1073/pnas.1304230110.
64. T. X. Dong *et al.*, T-cell calcium dynamics visualized in a ratiometric tdTomato-GCaMP6f transgenic reporter mouse. *ELife* **6**, e32417 (2017), 10.7554/eLife.32417.